Research Article

Journal of MASS SPECTROMETRY

Received: 12 January 2009 Accepted: 16 February 2009 Published online in Wiley Interscience: 30 March 2009

(www.interscience.com) DOI 10.1002/jms.1577

# Reaction diastereoselectivity of chiral aminoalcohols/$[Co(II)NO_3]^+$ complexes in evaporating ESI nanodroplets: new insights from a joint experimental and computational investigation

**Massimiliano Aschi,[a] Caterina Fraschetti,[b] Antonello Filippi,[b] and Maurizio Speranza[b]***

**The nature of the ionic species, formed by electrospray ionization (ESI) of $Co(NO_3)_2/CH_3OH$ solutions with a pair of aminoalcohols W and Y, has been investigated by mass spectrometric and computational methods. Collision induced dissociation (CID) of ions, formally corresponding to the $[WYCoNO_3]^+$ structures, yields fragmentation patterns which reflect not only the expected $[WYCoNO_3]^+$ connectivity but also that of other isomeric structures. Formation of these latter species is observed only in the presence of a tertiary aminoalcohol, like *N*-methylpseudoephedrine. The CID patterns are found to be strongly dependent on the chemical form (whether the free aminoalcohol or its hydrochloride), the configuration, and the relative concentration of the W and Y aminoalcohols. This variability parallels the results of classical MD (molecular dynamics) simulations of the $[WYCoNO_3]^+$ adducts which show a drastic alteration of the mechanical–dynamical features of the adducts by simply changing the charge state of W and/or Y, their absolute configuration, or by removing the solvent. The present experimental and computational study confirms the observation of fast stereoselective reactions in ESI nanodroplets before their evaporation and warns against any automatic correlation between the ESI spectrum of an analyte and its structure in solution.** 

*Supporting information may be found in the online version of this article.*

**Keywords:** diastereoselectivity; Co(II) complexes; chiral aminoalcohols; molecular dynamics; ESI-mass spectrometry

## Introduction

The stereospecific binding of metal ions to biomolecules may control their conformation as well as their chemical and biological properties. In this context, we have been interested in the coordination behaviour of ephedrines [either the (1S,2R)-(+)-enantiomer (**(+)-E**) or the (1R,2S)-(−)- one (**(−) -E**)] and (1S,2S)-(+)-*N*-methylpseudoephedrine (**(+)-P**) towards cobalt ions in the gas phase, under conditions where the conformational landscape and the reactivity of these supramolecular systems are not influenced by solvation and ion pairing effects.[1] In particular, we examined the collision induced fragmentation (CID) of ions nominally corresponding to the $[((+)\text{-}\mathbf{P})_2CoNO_3]^+$ aggregates (*m/z* 479) generated by electrospray ionization (ESI) of $Co(NO_3)_2/CH_3OH$ solutions of **(+)-P** containing variable amounts of either **(+)-E** or **(−)-E** or their hydrochlorides [(+)-**E**•HCl and (−)-**E**•HCl, respectively: Table 1].

We noticed that CID of *m/z* 479 yields a fragmentation pattern which reflects not only the expected connectivity of the $[((+)\text{-}\mathbf{P})_2CoNO_3]^+$ complex (Scheme 1, paths (a)), but also that of other isomeric structures (Scheme 1, paths (b)). More importantly, the relative abundances of the ionic fragments from paths (a) and (b) were found to be strongly dependent on the presence, the chemical form (whether the free aminoalcohol or its hydrochloride), the configuration, and the concentration of the ephedrine present in the electrosprayed solution. On the grounds of these observations, it was concluded that fast stereoselective reactions may actually occur in the ESI nanodroplets during evaporation yielding isomeric forms of the *m/z* 479 ions.

Since ESI-MS has become a routine and widely used analytical tool, it would be of extreme interest to consolidate this conclusion once for all.[2–6] Thus, unequivocal evidence must be provided about the strict correspondence between the observed fragments and the structure of their precursors and about the reactive species involved in their formation. To these purposes, our previous investigation[1] has now been extended to other ionic species from the same aminoalcohols as well as from different ones (Table 1) in order to establish unequivocally whether in these further cases

* *Correspondence to: Maurizio Speranza, Dipartimento di Chimica e Tecnologie del Farmaco, Università "La Sapienza", P.le Aldo Moro 5-00185 Roma, Italy. E-mail: maurizio.speranza@uniroma1.it*

a *Dipartimento di Chimica, Ingegneria Chimica e Materiali, Università dell'Aquila, 67010 Coppito, AQ, Italy*

b *Dipartimento di Chimica e Tecnologie del Farmaco, Università "La Sapienza", 00185 Roma, Italy*

 

Journal of MASS SPECTROMETRY

**Table 1.** Structures and symbols of the employed aminoalcohols

| Formula | a | b | c | d | Molecular weight | Symbol |
|---|---|---|---|---|---|---|
|  | $N(CH_3)_2$ | $CH_3$ | H | OH | 179.26 | **(+)-P** |
| | $CH_3$ | $NHCH_3$ | H | OH | 165.24 | **(+)-E** |
| | $NHCH_3$ | $CH_3$ | OH | H | 165.24 | **(−)-E** |
| | $CH_3$ | $NH_2CH_3{}^+Cl^-$ | H | OH | 201.70 | **(+)-E•HCl** |
| | $NH_2CH_3{}^+Cl^-$ | $CH_3$ | OH | H | 201.70 | **(−)-E•HCl** |
| | H | $NH_2$ | OH | H | 137.18 | **(+)-A** |
| | $NH_2$ | H | H | OH | 137.18 | **(−)-A** |
| | Ph | $NH_2$ | H | OH | 213.28 | **(+)-B** |
| | $NH_2$ | Ph | OH | H | 213.28 | **(−)-B** |
| | $N(C_2H_5)_2$ | $CH_3$ | H | OH | 207.31 | **(+)-D** |
| | H | $NHC(CH_3)_3$ | OH | H | 193.29 | **(+)-T** |
| | $NHC(CH_3)_3$ | H | H | OH | 193.29 | **(−)-T** |
| 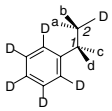 | D, $NHC(CH_3)_3$ | | D, OH | | 201.34 | **(±)-$d_8$-T** |

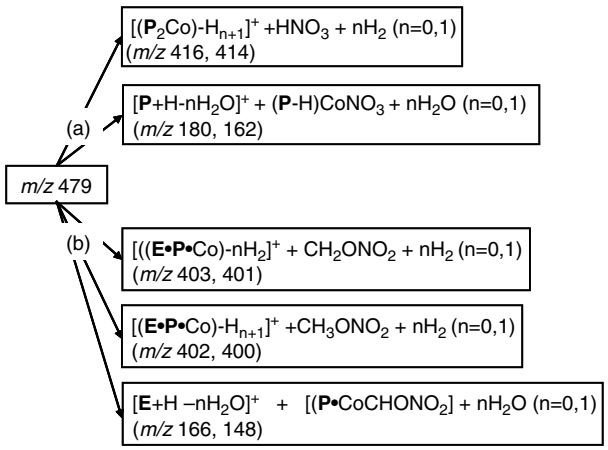


**Scheme 1.** Complete CID fragmentation pattern of the *m/z* 479 ion from electrosprayed **P**/**E** solutions ($E_{lab}$ = 5–20 eV). Paths (a) are attributed to the fragmentation of the $[\mathbf{P}_2\bullet CoNO_3]^+$ and/or $[(\mathbf{P}_2\text{-H})\bullet CoNO_3H]^+$ structures. Paths (b) are attributed to the fragmentation of the $[\mathbf{P}\bullet\mathbf{E}\bullet CH_2CoNO_3]^+$ and $[(\mathbf{P}\text{-H})\bullet\mathbf{E}\bullet CH_3CoNO_3]^+$ structures.

the connectivity of the ionic species from ESI does or does not correspond to that of their neutral precursors at equilibrium in solutions. In this respect, theoretical chemistry may, in principle, represent a powerful tool of investigation. However, in the present case, the matter seems too complicated for a straightforward application of the state-of-the-art computational strategies. A serious theoretical scenario should rely on a proper treatment of both desolvation and fragmentation processes which, in the typical mass-spectrometric conditions are conceivably dominated by dynamical, i.e. non-ergodic, effects. This means that any attempt, with the trivial exceptions of processes involving very small-sized systems, would be frustrated by the complexity of the problem.

Nevertheless, the above described experimental observation does indeed stimulate additional very intriguing questions. In particular, the sharp differences emerging from ESI experiments may be also produced by intrinsic, i.e. mechanical-thermodynamical differences between the investigated species. Therefore, we decided to analyze all the possible $[\mathbf{EP}CoNO_3]^+$ diastereomeric adducts by using classical molecular dynamics (MD) simulations, under equilibrium conditions both in ideal-gas phase and methanol solution. In this respect, the computational part of the present investigation is not aimed at elucidating the actual fragmentation mechanism but, rather, our primary goal is to evaluate more intrinsic physico–chemical differences between the different isomers to be eventually connected to experimental observations. More precisely our computational efforts are concentrated on the search of a plausible differential 'mechanical-fingerprint' which might play, if not the leading role, a not irrelevant part in the ESI patterns.

In the first part of this paper, precious information is provided on the origin of species like those responsible of paths (b) of Scheme 1, the requirements for their formation in ESI droplets, and the strict connection between their structure and their CID pattern. The second part of the paper, after an outline of preliminary Quantum–Mechanical (QM) calculations, is aimed at describing the underlying strategy and the results of MD simulations.

## Results and Discussion

### ESI-MS-CID experiments

We first tackled the problem of how reliable is the use of the CID pattern of a given ionic species to establish its connectivity. For instance, a sufficiently intense *m/z* 507 peak is detected from ESI of **P**/**T**/$Co(NO_3)_2$/$CH_3OH$ mixtures. After its isolation from accompanying ions in the first quadrupole of the instrument, the *m/z* 507 ion was allowed to collide with $N_2$ molecules in the second RF-only quadrupole and to fragment (CID). The CID fragmentation of the isolated *m/z* 507 ion {nominally corresponding to the $[\mathbf{T}_2CoNO_3]^+$ complex} *inter alia* leads to: *m/z* 444 (loss of $HNO_3$), *m/z* 431 (formal loss of $CH_2ONO_2$), *m/z* 194 ($\mathbf{T} + H^+$), and *m/z* 180 ($\mathbf{P} + H^+$). No significant effect of the **T** configuration on the relevant CID patterns is noticed. Although the loss of $HNO_3$ witnesses the expected occurrence of $[\mathbf{T}_2CoNO_3]^+$ {and its protomer $[(\mathbf{T}_2\text{-H})CoNO_3H]^+$}, the formal $CH_2ONO_2$ loss can be attributed to at least two isomeric structures, i.e. $[(\mathbf{P}\bullet\mathbf{T}\bullet CoCH_2ONO_2]^+$



  

(*m/z* 507), and $[(\mathbf{S} \bullet \mathbf{T}\bullet CoCH_2ONO_2]^+$ (*m/z* 507, **S** = α-isopropylaminomethyl)benzyl alcohol).

To discriminate between these two structures, the experiments were repeated by using $d_8$-**T**, instead of **T**. In this case, we detected two signals at *m/z* 523 and *m/z* 515, corresponding to $[(d_8\text{-}\mathbf{T})_2CoNO_3]^+$ (and its protomer), and $[(d_8\text{-}\mathbf{T} \bullet \mathbf{P}\bullet CoCH_2ONO_2]^+$ complexes, respectively. CID of *m/z* 523 does not produce any detectable amounts of *m/z* 447, which would be formed by formal elimination of $CH_2ONO_2$ from $[(d_8\text{-}\mathbf{S} \bullet d_8\text{-}\mathbf{T} \bullet CoCH_2ONO_2]^+$. Rather, it yields, besides *m/z* 202 ($d_8$-**T** + $H^+$), two other signals at *m/z* 460 and at *m/z* 457 which suggest the fragmentation sequence of Scheme 2. The loss of the $HNO_3$ fragment necessarily involves an intracomplex H shift, whereas the accompanying loss of HD requires the oxidation of the –CDOH– moiety of $d_8$-**T** to –CO–. The CID fragmentation of *m/z* 515 ions generates several fragment ions, including *m/z* 439, *m/z* 436, *m/z* 202 ($d_8$-**T** + $H^+$), and *m/z* 180 (**P** + $H^+$). Detection of these fragment ions confirms the occurrence of the $[d_8\text{-}\mathbf{T} \bullet \mathbf{P}\bullet CoCH_2ONO_2]^+$ structure and its fragmentation sequence (Scheme 3). The exclusive loss of HD further confirms what is mentioned earlier about the oxidation of the –CDOH– moiety of $d_8$-**T** to yield –CO–.

Having established the strict relationship between the CID patterns of isomeric binary complexes and their structures, we can now proceed to the analysis of the mechanism of their formation in ESI droplets. Besides the *m/z* 479 ion, nominally corresponding to the $[((+)\text{-}\mathbf{P})_2CoNO_3]^+$ structure, ESI of $Co(NO_3)_2/CH_3OH$ solutions containing **(+)-P** and **E** [i.e **(+)-E**, **(−)-E**, **(+)-E•** HCl, or **(+)-E•**HCl] leads to the formation of sufficiently intense *m/z* 465 peaks nominally corresponding to the $[\mathbf{E} \bullet (+)\text{-}\mathbf{P}\bullet CoNO_3]^+$ adducts. As shown in Scheme 4, an ion fragmentation pattern analogous to that of the *m/z* 479 companion (Scheme 1) was observed for the *m/z* 465 species, characterized by: (1) loss of $HNO_3$ (*m/z* 402); (2) formal loss of $CH_2ONO_2$ (*m/z* 389); (3) formal loss of $CH_3ONO_2$ (*m/z* 388); (4) formation of **P** + $H^+$ (*m/z* 180); and (5) formation of **E** + $H^+$ (*m/z* 166). As shown earlier for similar structures, fragment ions 1–3 are accompanied by their dehydrogenated forms, i.e. *m/z* 400, 387, and 386, respectively, whereas fragment ions 4 and 5 by their dehydrated forms, i.e. *m/z* 162 and 148, respectively. The pair of fragment ions differing for the loss of a hydrogen or a water molecule will be henceforth denoted by writing in italic the mass of the parent fragment ion, e.g. *m/z 402* for *m/z* 402 + *m/z* 400, and *m/z 180* for *m/z* 180 + *m/z* 162. The neutral species accompanying their formation will be denoted in italic as well [e.g. $HNO_3$ for the loss of $HNO_3$ (to give *m/z* 402) and of $HNO_3 + H_2$ (to give *m/z* 400 from *m/z* 465)].

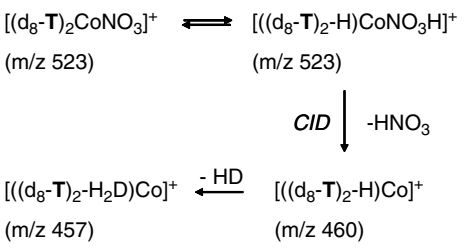


**Scheme 2.** Fragmentation sequence of the *m/z* 523 ion suggesting the occurrence of the $[(d_8\text{-}\mathbf{T})_2 \bullet CoNO_3]^+$ structure.

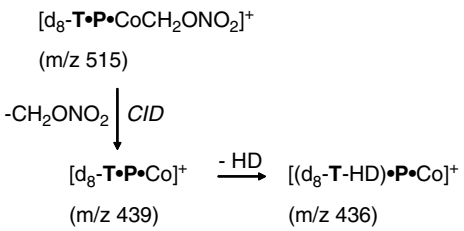


**Scheme 3.** Fragmentation sequence of the *m/z* 515 ion suggesting the occurrence of the $[d_8\text{-}\mathbf{T} \bullet \mathbf{P}\bullet CH_2CoNO_3]^+$ structure.

The combined relative abundances of each pair of fragment ions are given in Figs 1 and 2 as a function of the collision energy $E_{lab}$ (Fig. 1) and of the composition of the relevant mixtures at $E_{lab}$ = 15 eV (Fig. 2). As for *m/z* 479, CID of *m/z* 465 yields a fragmentation pattern which reflects not only the expected connectivity of the $[\mathbf{E} \bullet \mathbf{P}\bullet CoNO_3]^+$ complex (Scheme 4, paths (a)), but also that of other isomeric structures (Scheme 4, paths (b)). Their formation requires the transfer of a $CH_x$ (x = 2, 3) group to the nitrate moiety of the complex and the conversion of the **P** ligand to ephedrine or pseudoephedrine and/or that of the **E** ligand to norephedrine or norpseudoephedrine (**N** in Scheme 4).

At this point, another question arises: what is the $CH_x$ (x = 2, 3) group donor? Certainly, the **P** molecule. Indeed, a *m/z* 493 ion is formed in the ESI of the $Co(NO_3)_2/CH_3OH$ solutions with only **P**, whose CID pattern is dominated by the formal loss of $CH_2ONO_2$ (to give *m/z 417*) and $CH_3ONO_2$ (to give *m/z 416*).[1] This implies that both the $[\mathbf{P}_2CoCH_2ONO_2]^+$ and $[(\mathbf{P}_2\text{-H})CoCH_3ONO_2]^+$ isomers contribute to the *m/z* 493 ion. In contrast, no *m/z* 465 ion is observable in the ESI of the $Co(NO_3)_2/CH_3OH$ solutions with only **E** in any chemical form and configuration. This means that both **E** and **E•**HCl, as well as the solvent MeOH, are unable to transfer the $CH_x$ (x = 2, 3) group to the nitrate moiety of the complex to give the $[\mathbf{E}_2CoCH_2ONO_2]^+$ and $[(\mathbf{E}_2\text{-H})CoCH_3ONO_2]^+$ structures. Rather, the only binary complex formed in the ESI of **E**/$Co(NO_3)_2/CH_3OH$ solutions corresponds to *m/z* 451, whose CID pattern is only consistent with the expected $[\mathbf{E}_2CoNO_3]^+$ {or $[(\mathbf{E}_2\text{-H})CoNO_3H]^+$} structures.

On these grounds, it is concluded that the complexes, generated in the ESI of **E**/**P**/$Co(NO_3)_2/CH_3OH$ solutions, can undergo the $CH_x$ (x = 2, 3) group transfer only from **P** and not from **E** (or **E•**HCl) or the solvent MeOH. Furthermore, the observation that the ion patterns of both *m/z* 465 and *m/z* 479[1] dramatically depend on the configuration and the chemical form of ephedrine **E** in the **E**/**P**/$Co(NO_3)_2/CH_3OH$ mixtures lends strong support to the view of the $CH_x$ (x = 2, 3) transfer as taking place inside higher order complexes, e.g. $[(\pm)\text{-}\mathbf{E}\bullet ((+)\text{-}\mathbf{P})_2 \bullet CoNO_3]^+$, from a **P** ligand to the nitrate moiety. This view is supported by the observation that the ionic patterns from CID of *m/z* 465 are strongly sensitive to: (1) the specific form of ephedrine, whether as a neutral molecule or as the hydrochloride salt (cfr. e.g. **(+)-P**/**(+)-E** and **(+)-P**/**(+)-E•**HCl: Fig. 1); (2) the [**P**]/[**E**] concentration ratio (sol.1–sol.3 in Fig. 2); and (3) the specific configuration of ephedrine (cfr. e.g. **(+)-P**/**(+)-E** and **(+)-P**/**(−)-E**: Fig. 1).

Having identified the species involved in fast stereoselective reactions in the ESI nanodroplets from **E**/**P**/$Co(NO_3)_2/CH_3OH$ mixtures, we are now interested in checking whether the efficiency of these reactions depends on the structure and the electronic properties of the aminoalcoholic ligands. To this purpose, we investigated the CID of the binary complexes formed in the ESI of $Co(NO_3)_2/CH_3OH$ mixtures with the other aminoalcohols listed in Table 1 (generically denoted as W and Y in Table 2). 'No' in Table 2 means that the CID pattern of the relevant binary complex is exclusively consistent with the $[WYCoNO_3]^+$ structure

Journal of MASS SPECTROMETRY

{or its $[(WY\text{-}H)CoNO_3H]^+$ protomer}. In contrast, 'yes' indicates that formation of the $[WYCoNO_3]^+$ structure is always accompanied by the $[(WY\text{-}(x\text{-}2)H)CoCH_2ONO_2]^+$ (x = 2, 3) ones.

For instance, as said before, CID of *m/z* 507 from $Co(NO_3)_2/CH_3OH$ mixtures containing **(+)-P** and either **(+)-T** or **(−)-T** are consistent with both the $[(\mathbf{T}_2\text{-}H)CoNO_3H]^+$ (*m/z 444* by formal loss of $HNO_3$) and the $[\mathbf{P}\bullet(\mathbf{T}\text{-}H)\bullet CoCH_2ONO_2]^+$ (*m/z 431* by formal loss of $CH_2ONO_2$). In contrast, no signals corresponding to *m/z 431* were detected in the CID spectra of the *m/z* 507 ion, when electrosprayed from mixtures containing only **T**, thus indicating the exclusive occurrence of the $[\mathbf{T}_2CoNO_3]^+$ complex {or its $[(\mathbf{T}_2\text{-}H)CoNO_3H]^+$ protomer}. The intracomplex $CH_x$ (x = 2, 3) group transfer is not only observed in electrosprayed W/**P**/$Co(NO_3)_2/CH_3OH$ solutions with W = **E**, **P**, or **T**, but it can be detected in solution containing primary aminoalcohols, like W = **A** or **B**. Instead, the same reaction does not take place in the complexes from ESI of **P**/$Co(NO_3)_2/CH_3OH$ mixtures with another tertiary aminoalcohol, i.e. **D** (Table 2). The full scan of the ESI-MS of **D**/**P**/$Co(NO_3)_2/CH_3OH$ mixture is characterized by the presence of moderate amounts of *m/z* 493 (nominally corresponding to $[\mathbf{P}_2CoCH_2ONO_2]^+$) and by the complete absence of the *m/z* 521 and *m/z* 549 {corresponding to $[\mathbf{D}_x \bullet \mathbf{P}_{(2-x)} \bullet CoCH_2ONO_2]^+$ (x = 1, 2)}. Besides, CID of a signal at *m/z* 507 is consistent with the $[\mathbf{D} \bullet \mathbf{P}\bullet CoNO_3]^+$ connectivity, and not with the $[\mathbf{P}_2CoC_2H_4ONO_2]^+$ one. Analogously, CID of a signal at *m/z* 535 is consistent with the $[\mathbf{D}_2CoNO_3]^+$ structure, and not with the $[\mathbf{D} \bullet \mathbf{P}\bullet CoC_2H_4ONO_2]^+$ one. Finally, no peaks at *m/z* 563 {nominally corresponding to $[\mathbf{D}_2CoC_2H_4ONO_2]^+$} are detected.

All these observations can be summarized as follows:

(1) An intracomplex $CH_x$ (x = 2, 3) group transfer takes place in ESI nanodroplets which is promoted by ionization of the ligand tertiary amino group of **P**. If actually accessible, ionization of secondary (in the **E** and **T** ligands) or primary amino groups (in the **A** and **B** ligands) tend to transfer the proton rather than the $CH_x$ (x = 2, 3) group. Therefore, to observe an intracomplex $CH_x$ (x = 2, 3) group transfer, the presence of a tertiary aminoalcohol is essential.

(2) The results obtained in the **D**/**P**/$Co(NO_3)_2/CH_3OH$ mixtures indicate that the intracomplex $CH_x$ (x = 2, 3) group transfer from **P** is inhibited by the presence of the **D** ligand in the complex. This effect can be explained by considering that the $N(C_2H_5)_2$ of **D** is more easily ionizable than the $N(CH_3)_2$

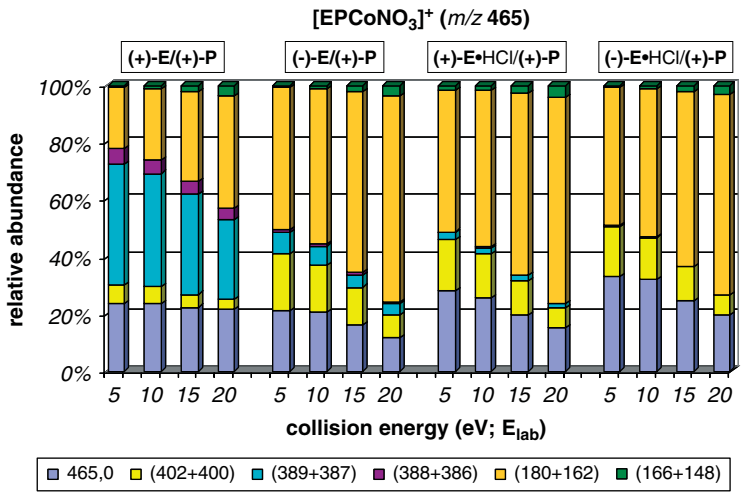


**Figure 1.** Relative abundance of the fragment ions from CID of *m/z* 465 from [**P**]/[**E**] = 1 as a function of the collision energy ($E_{lab}$).

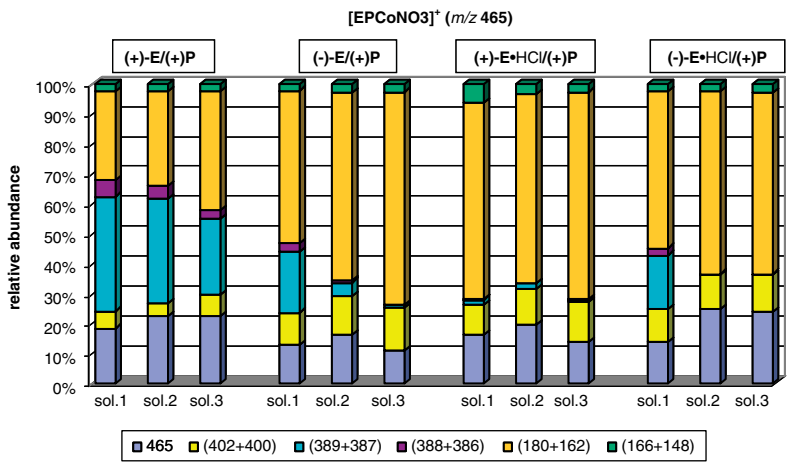


**Figure 2.** Relative abundance of the fragment ions from CID ($E_{lab}$ = 15 eV) of *m/z* 465 as a function of the relative concentrations of **E** and **P** in the electrosprayed solution {[**P**]/[**E**] = 0.5 (sol. 1); 1.0 (sol. 2); 2.0 (sol. 3)}.



  

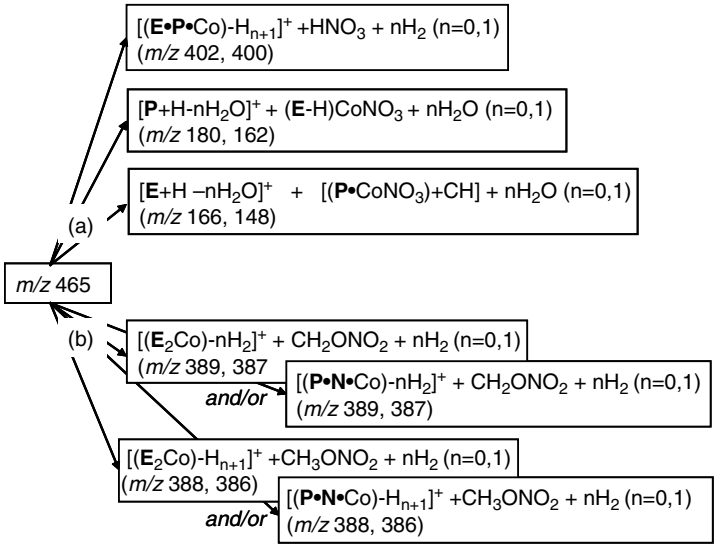


**Scheme 4.** Complete CID fragmentation pattern of the *m/z* 465 ion from electrosprayed **P**/**E** solutions ($E_{lab}$ = 5–20 eV). Paths (a) are attributed to the fragmentation of the [**P**•**E**•$CoNO_3$]$^+$ and/or [(**P**-H)•**E**•$CoNO_3H$]$^+$ structures. Paths (b) are attributed to the fragmentation of the [**E**$_2$•$CH_2CoNO_3$]$^+$ and [(**E**$_2$-H)•$CH_3CoNO_3$]$^+$ structures.

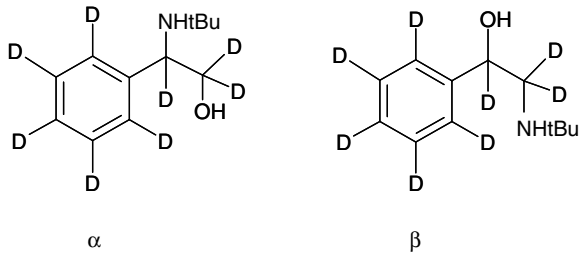


**Scheme 5.** Structures of the $\alpha$ and $\beta$ regioisomers formed in the synthesis of (±)-d$_8$-**T**.[11].

**Table 2.** Formation of [(WY-(x-2)H)$CoCH_xNO_3$]$^+$ (x = 2, 3) structures from ESI of W/Y/$Co(NO_3)_2$/$CH_3OH$ solutions ([W]/[Y] = 1)

| | Aminoalcohol W | | | | | |
|---|---|---|---|---|---|---|
| Aminoalcohol Y | **E** | **P** | **T** | **A** | **B** | **D** |
| **E** | No | Yes | No | – | – | – |
| **P** | Yes | Yes | Yes | Yes | Yes | No |
| **T** | No | Yes | No | – | No | – |
| **A** | – | Yes | | No | | – |
| **B** | – | Yes | No | – | No | – |
| **D** | – | No | – | – | – | – |

of **P** (For instance, ionization potentials *IP*(eV molecule$^{-1}$) ($N(C_2H_5)_3$ = 7.53 < $(CH_3)_2NC_2H_5$) = 7.74 eV); proton affinity *PA*(kcal mol$^{-1}$) ($N(C_2H_5)_3$ = 234.7 > $(CH_3)_2NC_2H_5$) = 229.5)[7]. This minimizes any conceivable $CH_2$ group transfer from **P** in favour of the elimination of ethylene from the ionized $N(C_2H_5)_2$ moiety induced by proton interaction with the $NO_3$ moiety.

(3) The general decrease in reactivity with **E**H$^+$Cl$^-$, instead of the free base **E**, is attributed to the presence of the $NH_2CH_3^+$ group of **E** in the complexes. Indeed, the $CH_x$ (x = 2, 3) group transfer from a conceivably ionized **P** would be preceded by a fast proton transfer from the $NH_2CH_3^+$ group.

In conclusion, CID spectra of the binary ions at *m/z* 479 and *m/z* 465, formed by ESI of $Co(NO_3)_2$/$CH_3OH$ solutions with either pure **(+)-P** or its mixtures with **(+)-E** or **(−)-E**, provide indirect evidence of stereoselective $CH_x$ migration within high-order aggregates during solvent evaporation of the ESI nanodroplets. The CID spectra of d$_8$-**T**/**P**/$Co(NO_3)_2$ solutions allow us to discriminate between [(d$_8$-**T**)$_2$$CoNO_3$]$^+$ and [**P** • d$_8$-**T** • $CoCH_2ONO_2$]$^+$, thus confirming the strict correspondence of the CID patterns with the complex connectivities. Furthermore, the experimental results identify **P** as the $CH_x$-donor, indicating that a tertiary aminoalcohol is essential. An activating ionization of the donor is necessary, although its protonation can favour the faster proton transfer. This view is confirmed by the observation that, with the more easily ionizable **D** ligand, any intracomplex alkyl group transfer is inhibited by a faster ethylene elimination, leading to the loss of $C_2H_4$ and $HNO_3$.

## Theoretical calculations

Classical MD simulations do represent a very powerful tool of investigation provided a reliable force field is available. This point has been tackled in the present study by using Density Functional Theory (DFT) calculations (see Experimental Section for the details). We focussed our attention on the [(−)-**E**•(+)-**P**•$CoNO_3$]$^+$ adducts considering both the doublet and quartet electron state and all the conceivable covalent frameworks, namely neutral, mono-, and bis-zwitterionic, schematically shown in Fig. 3. Then, the [(−)-**E**•(+)-**P**•$CoNO_3$]$^+$ force field parameters have been exported to all [(+)-**E**•(+)-**P**•$CoNO_3$]$^+$ adducts.

Results, briefly collected in Table 3, clearly indicate that, irrespective of the covalent framework, the [(−)-**E**•(+)-**P**•$CoNO_3$]$^+$ adducts preferentially adopt a quartet state in the gas phase. The very large energy differences with doublet state also suggest that quartet species should represent the most abundant, if not the unique, magnetic state also in solution. This finding prompted us to use, as force field for the present study, the atomic charges

Journal of MASS SPECTROMETRY

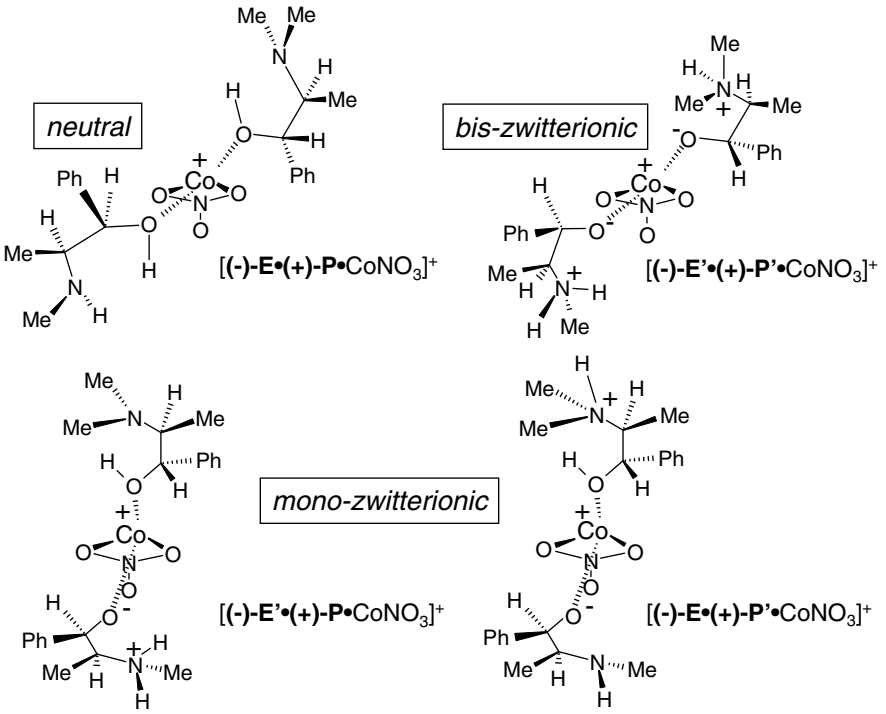


**Figure 3.** Schematic view of the covalent frameworks utilized for MD simulations.

**Table 3.** B3LYP/BS (BS: LANL2DZ on Co, 6-31G* on others) relative energies (at 0 K) of the species reported in Figure 3

| Species | | ΔE (kcal/mol) |
|---|---|---|
| **[(−)-E•(+)-P•CoNO$_3$]$^+$** | doublet | 20.5[a] |
| | quartet | 8.5 |
| **[(−)-E′ • (+)-P•CoNO$_3$]$^+$** | doublet | 14.4 |
| | quartet | 3.9[a] |
| **[(−)-E•(+)-P′•CoNO$_3$]$^+$** | doublet | 12.7 |
| | quartet | 1.5 |
| **[(−)-E′ • (+)-P′•CoNO$_3$]$^+$** | doublet | 12.7 |
| | quartet | 0.0 |

[a] Not fully optimized

of the quartet species with all the rest of the parameters, i.e. Lennard-Jones, stretching, bending, and torsional, taken from the Gromos96 force field.[8] The above parameters were finally optimized by reproducing the DFT gas phase quartet energy differences of Table 3.

MD simulations were carried out at 300 K both in gas phase and in methanol solution at the typical density of 792 kg/m$^3$ at 1 bar of pressure (see Experimental section for the details). For each adduct, we simulated the neutral {[(−)-**E**•(+)-**P**•CoNO$_3$]$^+$, [(+)-**E**•(+)-**P**•CoNO$_3$]$^+$}, the bis-zwitterionic {[(−)-**E**′•(+)-**P**′•CoNO$_3$]$^+$, [(+)-**E**′•(+)-**P**′•CoNO$_3$]$^+$} and the two mono-zwitterionic {[(−)-**E**′•(+)-**P**•CoNO$_3$]$^+$, [(+)-**E**′ • (+)-**P**•CoNO$_3$]$^+$, [(−)-**E**•(+)-**P**′•CoNO$_3$]$^+$, [(+)-**E**•(+)-**P**′•CoNO$_3$]$^+$} species for a total of eight simulations in gas phase and eight in methanol solution (the zwitterionic forms of **E** and **P** are respectively denoted as **E**′ and **P**′).

At a first sight, all the simulated adducts show a rather high flexibility making the above structures, obtained from QM calculations, rather poorly representative of the system. From this preliminary observation it immediately emerges the importance of a MD-based approach for better addressing the problem at hand. Moreover all the species turn out to be characterized by a very similar mechanical fingerprint in which the $CoNO_3$ moiety appears very rigid with all the fluctuation pattern concentrated within **E** and **P** groups. In particular **E** and **P** roughly show two kinds of motions: (1) a 'rigid-body' rotating motion with respect $CoNO_3$ moiety and (2) internal fluctuations, e.g. mutual rotation of phenyl and amino groups. Essential dynamics[9] was employed to obtain a more quantitative and systematic comparison of the overall mechanical properties of the investigated systems. This method is based on the construction of the covariance matrix, C, of the positional deviations of the atoms along the trajectories (note that in our simulations the roto-translations have been removed and all the structures are least-squared fitted). The symmetric matrix C, when diagonalized, provides a set of eigenvectors ($\eta$) representing the directions in the configurational space along which the system fluctuates. The sum of the eigenvalues, i.e. the trace associated to each eigenvector provides the extent of the fluctuation along the above directions, i.e. the flexibility of the systems reported in Table 4.

The results indicate that the adducts undergo a change of flexibility upon variation of the covalent framework and systematically become more confined, i.e. more rigid, when passing from gas phase to methanol solution. At the same time, all the investigated systems show a rather steep spectrum of eigenvalues showing only two values significantly different from zero which, therefore, are sufficient to describe the overall mechanical–dynamical properties of the adducts. This finding allowed us to better characterize the MD results by projecting all the trajectories onto the plane described such eigenvectors offering a geometrically simple representation. For the sake of clarity we show, in Fig. 4, the result of the above procedure for



  

**Table 4.** Trace of the diagonalized all-atom covariance matrix for all of the investigated species

| Species | Solvent | Trace ($nm^2$) |
|---|---|---|
| **[(−)-E•(+)-P•CoNO$_3$]$^+$** | None | 1.0 |
| | Methanol | 0.5 |
| **[(+)-E•(+)-P•CoNO$_3$]$^+$** | None | 0.7 |
| | Methanol | 0.6 |
| **[(−)-E′ • (+)-P′ • CoNO$_3$]$^+$** | None | 1.2 |
| | Methanol | 0.4 |
| **[(+)-E′ • (+)-P′ • CoNO$_3$]$^+$** | None | 1.1 |
| | Methanol | 0.5 |
| **[(−)-E′ • (+)-P•CoNO$_3$]$^+$** | None | 1.3 |
| | Methanol | 0.4 |
| **[(+)-E′ • (+)-P•CoNO$_3$]$^+$** | None | 1.1 |
| | Methanol | 0.6 |
| **[(−)-E•(+)-P′ • CoNO$_3$]$^+$** | None | 1.0 |
| | Methanol | 0.5 |
| **[(+)-E•(+)-P′ • CoNO$_3$]$^+$** | None | 1.2 |
| | Methanol | 0.6 |

one adduct (with both **(−)-E** and **(+)-P** in neutral form, with all the others reported in the Supporting Information) in gas phase and in methanol.

The spots appearing in the figure, corresponding to a non-zero probability to find the molecule around a given geometry, indicate that the [(−)-**E**•(+)-**P**•CoNO$_3$]$^+$ adduct is characterized by different conformers, separated by relatively high barriers (lack of spots) in gas phase and in rapid mutual equilibrium (lack of discontinuity) in methanol. It follows that the solvent, beyond the previously mentioned mechanical hindrance, also leads the system to a different conformational sampling. To quantitatively evaluate the mechanical–dynamical differences between the two simulations, i.e. gas phase *versus* methanol for the case reported in Fig. 4, we calculated and compared the extent of the overlap between the corresponding eigenvectors $\eta$ by using the Root Mean Square Inner Product (RMSIP) formula:[10]

$$\mathrm{RMSIP} = \left( \frac{\sum_{i=1}^{N} \sum_{j=1}^{N} (\eta_i^A \bullet \eta_j^B)^2}{N} \right)^{1/2}$$

where *A* and *B* indicate two generic systems and *N* the dimension of the covariance matrix (i.e. equal to 3N if all the *N* atoms are considered). The obtained value equal to 0.19, much lower than unity, unequivocally points out the poor overlap between the two conformational spaces, i.e. very different mechanical–dynamical features sharply indicating that the solvent produces not only a geometrical but also a mechanical–dynamical differential effect.

In order to extend the latter findings also to the other adducts, we calculated the above overlap between the eigenvectors of gaseous and methanolic [(−)-**E**•(+)-**P**•CoNO$_3$]$^+$ with the ones of all the other species. The results, collected in Table 5, confirm the previous trend. Note that the same analysis carried out for all the species provide the same qualitative scenario, i.e. RMSIP never exceeding 0.4.

Therefore, a drastic alteration of the mechanical–dynamical features of the adduct is observed by simply changing the charge state of **E** and/or **P** or the absolute configuration of **E** or by removing the solvent. This somewhat surprising result, although not explaining, may partially justify the differences experimentally detected in the ESI-MS-CID fragmentation patterns of [**E** • **P**•CoNO$_3$]$^+$. As a matter of fact, even neglecting the important dynamical effects of non-equilibrium conditions, the sharp differences emerged at the equilibrium can somehow play an important role in the fragmentation dynamics. Unfortunately, the complexity of the investigated systems does not allow, at the moment, a more direct structure–activity relationship. Finally. it must be also stressed that, at room temperature, both in the gas

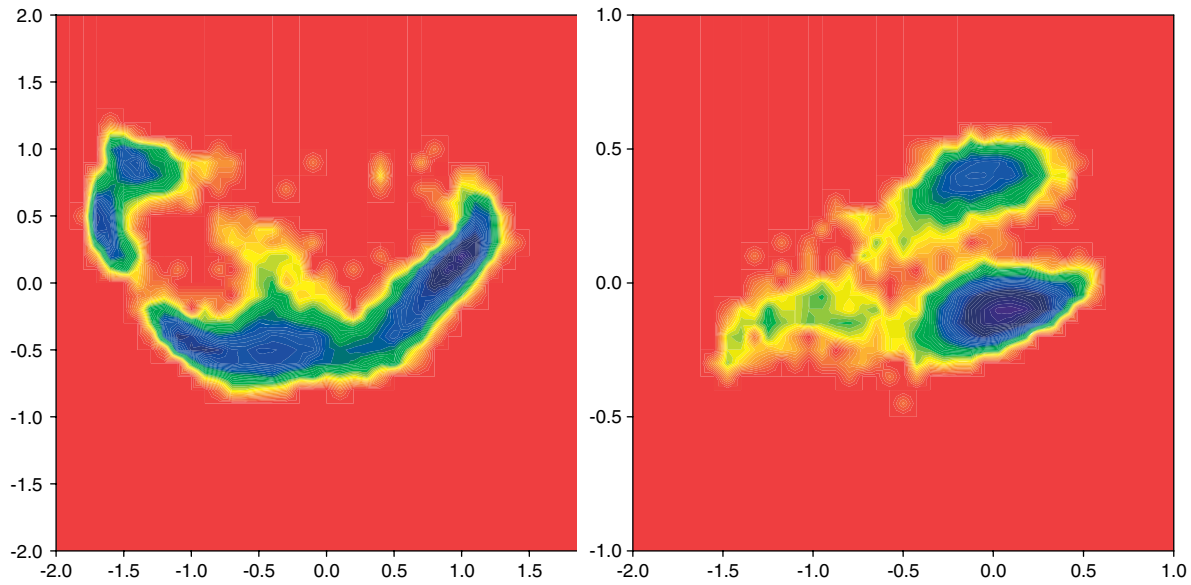


**Figure 4.** Projection of the MD simulations onto the plane formed by the first two essential eigenvectors for [(−)-**E**•(+)-**P**•CoNO$_3$]$^+$ adduct in methanol (left side panel) and gas phase (right side panel) (units are in nanometre).

Journal of MASS SPECTROMETRY

**Table 5.** RMSIP between neutral [(−)-**E**(+)-**P**$CoNO_3$]$^+$ adducts in gas (*g*) and methanol (*m*) phase and all the other investigated species

| Species | | [(−)-**E**(+)-**P**$CoNO_3$]$^+$ Gas (*g*) | Methanol (*m*) |
|---|---|---|---|
| **[(+)-E•(+)-P•CoNO$_3$]$^+$** | *g* | 0.31 | 0.25 |
| **[(+)-E•(+)-P•CoNO$_3$]$^+$** | *m* | 0.19 | 0.32 |
| **[(−)-E′ • (+)-P′•CoNO$_3$]$^+$** | *g* | 0.20 | 0.27 |
| **[(−)-E′ • (+)-P′•CoNO$_3$]$^+$** | *m* | 0.25 | 0.16 |
| **[(+)-E′ • (+)-P′•CoNO$_3$]$^+$** | *g* | 0.31 | 0.19 |
| **[(+)-E′ • (+)-P′•CoNO$_3$]$^+$** | *m* | 0.13 | 0.34 |
| **[(−)-E′ • (+)-P•CoNO$_3$]$^+$** | *g* | 0.10 | 0.21 |
| **[(−)-E′ • (+)-P•CoNO$_3$]$^+$** | *m* | 0.15 | 0.19 |
| **[(+)-E′ • (+)-P•CoNO$_3$]$^+$** | *g* | 0.25 | 0.10 |
| **[(+)-E′ • (+)-P•CoNO$_3$]$^+$** | *m* | 0.12 | 0.14 |
| **[(−)-E•(+)-P′•CoNO$_3$]$^+$** | *g* | 0.24 | 0.23 |
| **[(−)-E•(+)-P′•CoNO$_3$]$^+$** | *m* | 0.25 | 0.25 |
| **[(+)-E•(+)-P′•CoNO$_3$]$^+$** | *g* | 0.14 | 0.32 |
| **[(+)-E•(+)-P′•CoNO$_3$]$^+$** | *m* | 0.31 | 0.14 |

phase and in solution, the systems may exist in a large number of conformations in mutual equilibrium. This obvious consideration poses a severe question as to whether it makes sense to use static QM calculations, without thermal or dynamical effects, to provide semi-quantitative explanations to the unimolecular reactivity under mass spectrometric conditions.

## Experimental section

### *Materials*

Enantiomerically pure compounds (1S,2S)-(+)-*N*-methylpseudoephedrine (**(+)-P**), (1S,2R)-(+)-ephedrine hydrochloride (**(+)-E•**HCl), (1R,2S)-(−)-ephedrine hydrochloride (**(−)-E•**HCl), (1R,2S)-(−)-ephedrine (**(−)-E**), (S)-(+)-2-amino-1-phenylethanol (**(+)-A**), (R)-(−)-2-amino-1-phenylethanol (**(−)-A**), (1S,2R)-(+)-2-amino-1,2-diphenylethanol (**(+)-B**), (1R,2S)-(−)-2-amino-1,2-diphenylethanol (**(−)-B**), (1S,2S)-(+)-diethylnorpseudoephedrine (**(+)-D**), (S)-(+)-2-*tert*-butylamino-1-phenylethanol (**(+)-T**), and (R)-(−)-2-*tert*-butylamino-1-phenylethanol (**(−)-T**) were purchased from a commercial source and used without further purification. **(+)-E** was obtained by treatment of corresponding hydrochloride with $NaHCO_3$ saturated aqueous solution.

A simple and safe procedure was used to prepare the racemic mixture of (±)-$d_8$-**T**:[11] 3 mmol of *tert*-butylamine was added dropwise to a stirred solution of commercially available $d_8$-styrene epoxide (2.5 mmol) in 1 ml of water. The mixture was stirred for about 14 h at room temperature. After addition of 1 ml of water, the organic materials were extracted with diethyl ether (2 × 5 ml) and dried over anhydrous $Na_2SO_4$. The crude product was analyzed by $^1$H-NMR (yield, 80%; ratio $\alpha : \beta$ regioisomers, 10 : 90 (Scheme 5)).

*Mass spectrometric experiments.* The ESI-MS-CID experiments were performed on an Applied Biosystems Linear Ion Trap (LIT) API 2000 mass spectrometer equipped with an ESI source and a syringe pump. The aminoalcohols of interest were added to methanolic solutions of $Co(NO_3)_2$ ($1 \times 10^{-4}$ M). The overall concentration of the aminoalcohols was $4 \times 10^{-4}$ M. Operating conditions of the ESI source are as follows: ion spray voltage = +5.5 kV; sheath gas = 34 psi; nebulizer gas = 15 psi; focusing rod offset (IS) = +10 V; orifice plate = +35 V; capillary temperature = 210 °C. Methanolic solutions are infused via a syringe pump at a flow rate of 10 µl/ min. CID experiments are performed in the following way: after isolation in the first quadrupole, precursor ions are allowed to go through the collision region, where their CID takes place. The survivor precursor and its product ions were accumulated in the LIT of the instrument (fill time of the trap = 20 ms; scan rate = 1000 amu/s) to improve the signal-to-noise ratio and eventually detected. Operating conditions in CID experiments are: nominal pressure of nitrogen in collision chamber, $1,4 \times 10^{-5}$ torr; the CID collision energy (in eV; lab frame) is calculated from the potential difference between IS and collision cell rod offset. The relative abundance of fragment ions results from peak integration from the spectra acquired in profile mode. In each acquisition the final spectra are the average of about 70 scans, each consisting of two microscans. The standard deviation of the relative ion abundances is about ±10%.

### *Computational details*

QM calculations (geometry optimization and atomic charges) were performed using the Gaussian 03 suite of programmes[12] installed on dual processor Opteron workstations. The calculations were carried out at the B3LYP[13] level of theory using the 6-31G* basis set for H, C, N, O, and the LANL2DZ[14] one for Co.

A modified version of Gromacs package[14] was used for producing all the MD trajectories in the number pf particles at constant volume and temperature (NVT) ensemble.[15] All the systems, after an initial mechanical relaxation and (if present) solvent equilibration, were slowly heated using short trajectories of 50 ps length from 50 to 300 K. After a few nanosecond of equilibration 20 ns of simulation were produced at 300 K. A time step of 2 fs was adopted and the rototranslational motion was removed,[16] the temperature was kept fixed at 300 K by the isokinetic temperature coupling[17] and the long-range electrostatics was treated by means of the Particle Mesh Ewald method.[18] All the subsequent analyses were carried out using standard Gromacs tools or using home-made routines.

## Acknowledgements

Financial supports by Università 'Sapienza', Roma, Italy (Funds for selected research topics 2008-2010) and PRIN grant n. 2007H9S8SW_002 (MIUR) are acknowledged.

## Supporting information

Supporting information may be found in the online version of this article.

## References

[1] C. Fraschetti, M. Aschi, A. Filippi, A. Giardini, M. Speranza. Fast stereoselective reactions in electrosprayed Co(ii)/neurotransmitter nanodroplets. *Chemical Communications* **2008**, *22*, 2544.
[2] P. Nemes, S. Goyal, A. Vertes. Conformational and noncovalent complexation changes in proteins during electrospray ionization. *Analytical Chemistry* **2008**, *80*, 387.
[3] C. L. Sherman, J. S. Brodbelt. An Equilibrium partitioning model for predicting response to host-guest complexation in electrospray ionization mass spectrometry. *Analytical Chemistry* **2003**, *75*, 1828.



  

[4] J. E. Ham, B. Durham, J. R. Scott. Design of instrumentation for probing changes in electrospray droplets via the Stern-Volmer relationship. *The Review of Scientific Instruments* **2005**, *76*, 014101/1.
[5] R. L. Grimm, J. L. Beauchamp. Dynamics of field-induced droplet ionization: Time-Resolved studies of distortion, jetting, and progeny formation from charged and neutral methanol droplets exposed to strong electric fields. *Journal of Physical Chemistry B* **2005**, *109*, 8244.
[6] Z. Tian, S. R. Kass. *J.* Does electrospray ionization produce gas-phase or liquid-phase structures? *Journal of the American Chemical Society* **2008**, *130*, 10 842; See, also: Z. Tian, S. R. Kass. *J.* Gas-phase versus liquid-phase structures by electrospray ionization mass spectrometry. *Angewandte Chemie International Edition* **2009**, *48*, 1321.
[7] http://webbook.nist.gov/chemistry/.
[8] W. F. van Gunsteren, S. R. Billeter, A. A. Eising, P. H. Hunenberger, P. Kruger, A. Mark, W. R. P. Scott, I. G. Tironi. *Biomolecular Simulation: The GROMOS96 Manual and User Guide*. vdf Hochschuleverlag AG an der ETH Zurich and BIOMOS b.v.: Zurich, Groningen, **1996**.
[9] A. Amadei, B. M. Linssen, H. J. C. Berendsen. Essential dynamics of proteins. *Proteins: Structure, Function and Genetics* **1993**, *17*, 412.
[10] A. Amadei, M. Ceruso, A. Di Nola. On the convergence of the conformational coordinates basis set obtained by the essential dynamics analysis of proteins' molecular dynamics simulations. *Proteins: Structure, Function and Genetics* **1999**, *36*, 419.
[11] N. Azizi, M. R. Saidi. Highly Chemoselective Addition of Amines to Epoxides in Water. *Organic Letters* **2005**, *7*, 3649.
[12] M. J. Frisch, G. W. Trucks, H. B. Schlegel, G. E. Scuseria, M. A. Robb, J. R. Cheeseman, J. A. Montgomery Jr, T. Vreven, K. N. Kudin, J. C. Burant, J. M. Millam, S. S. Iyengar, J. Tomasi, V. Barone, B. Mennucci, M. Cossi, G. Scalmani, N. Rega, G. A. Petersson, H. Nakatsuji, M. Hada, M. Ehara, K. Toyota, R. Fukuda, J. Hasegawa, M. Ishida, T. Nakajima, Y. Honda., O. Kitao., H. Nakai., M. Klene, X. Li, J. E. Knox, H. P. Hratchian, J. B. Cross, C. Adamo, J. Jaramillo, R. Gomperts, R. E. Stratmann, O. Yazyev, A. J. Austin, R. Cammi, C. Pomelli, J. W. Ochterski, P. Y. Ayala, K. Morokuma, G. A. Voth, P. Salvador, J. J. Dannenberg, V. G. Zakrzewski, S. Dapprich, A. D. Daniels, M. C. Strain, O. Farkas, D. K. Malick, A. D. Rabuck, K. Raghavachari, J. B. Foresman, J. V. Ortiz., Q. Cui., A. G. Baboul., S. Clifford., J. Cioslowski, B. B. Stefanov, G. Liu, A. Liashenko, P. Piskorz, I. Komaromi, R. L. Martin, D. J. Fox, T. Keith, M. A. Al-Laham, C. Y. Peng, A. Nanayakkara, M. Challacombe, P. M. W. Gill, B. Johnson, W. Chen, M. W. Wong, C. Gonzalez, J. A. Pople. *Gaussian 03. Revision C.02*. Gaussian. Inc.: Wallingford CT, **2004**.
[13] (a) A. D. Becke. A new mixing of Hartree-Fock and local-density-functional theories. *Journal of Chemical Physics* **1993**, *98*, 1372, Density-functional thermochemistry. III. The role of exact exchange. 5648; (b) C. Lee, W. Yang, R. G. Parr. Development of the Colle-Salvetti correlation-energy formula into a functional of the electron density. *Physical Review B* **1988**, *37*, 785.
[14] P. J. Hay, W. R. Wadt. Ab initio effective core potentials for molecular calculations. Potentials for potassium to gold including the outermost core orbitals. *Journal of Chemical Physics* **1985**, *82*, 299.
[15] H. J. van der Spoel, A. R. Berendsen, M. E. F. van Buuren, P. J. M. Apol, A. L. T. M. Sijbers. *GROMACS User Manual*. University of Groningen: Groningen, The Netherlands, **1995**.
[16] A. Amadei, G. Chillemi, M. A. Ceruso, A. Grottesi, A. Di Nola. Molecular dynamics simulations with constrained roto-translational motions: Theoretical basis and statistical mechanical consistency. *Journal of Chemical Physics* **2000**, *112*, 9.
[17] D. J. Evans, G. P. Morris. *Statistical Mechanics of Nonequilbrium Liquids*. Academic Press: London, **1990**.
[18] T. Darden, D. York, L. Pedersen. Particle mesh Ewald: an N log(N) method for Ewald sums in large systems. *Journal of Chemical Physics* **1993**, *98*, 10 089.

  